Aptamer photoregulation in vivo

Lele Li[a,b,c,1], Rong Tong[a,b,c,1], Hunghao Chu[a,b,c], Weiping Wang[a,b,c], Robert Langer[b,c,2], and Daniel S. Kohane[a,2]

[a]Laboratory for Biomaterials and Drug Delivery, Department of Anesthesiology, Division of Critical Care Medicine, Children's Hospital Boston, Harvard Medical School, Boston, MA 02115; and [b]Department of Chemical Engineering and [c]Koch Institute for Integrative Cancer Research, Massachusetts Institute of Technology, Cambridge, MA 02139

Contributed by Robert Langer, October 21, 2014 (sent for review July 31, 2014)

The in vivo application of aptamers as therapeutics could be improved by enhancing target-specific accumulation while minimizing off-target uptake. We designed a light-triggered system that permits spatiotemporal regulation of aptamer activity in vitro and in vivo. Cell binding by the aptamer was prevented by hybridizing the aptamer to a photo-labile complementary oligonucleotide. Upon irradiation at the tumor site, the aptamer was liberated, leading to prolonged intratumoral retention. The relative distribution of the aptamer to the liver and kidney was also significantly decreased, compared to that of the free aptamer.

aptamer | light triggering | cancer targeting

Aptamers are single-stranded nucleic acids that have emerged as a promising class of therapeutics owing to their relative ease of synthesis and high affinity and selectivity toward a range of targets including small molecules, proteins, viral particles, and living cells (1–6). Aptamers can fold into well-defined conformations and are more resistant to enzymatic degradation than other oligonucleotides (7–9). Aptamers have been suggested for imaging applications because their relatively small size and molecular mass (~10 kDa) allow fast tissue penetration and clearance from blood (10, 11). The same characteristics make aptamers promising for effective delivery of diagnostic and therapeutic agents to tissues or organs. However, nonspecific accumulation of aptamers in normal tissues is undesirable (12–15) because it diminishes the proportion of aptamer that targets the desired tissue. This can adversely affect the therapeutic index of the aptamer; this may be particularly true if the aptamer is conjugated to a drug or drug delivery device. Moreover, aptamers themselves can have nonspecific toxic effects (16, 17). Ideally aptamers would achieve a high concentration in a pathological tissue of interest while maintaining low levels elsewhere. The activity of aptamers can be modulated in vivo by binding to polymers or complementary oligonucleotide sequences (18–20), but spatiotemporal regulation of aptamer activity in vivo has not been achieved, whereby activity would be enhanced in target tissues and not others. Here, we report a strategy to provide light-triggered control of aptamer function and distribution in vivo.

Light is an excellent means of providing external spatiotemporal control of biological systems (21–26). Many strategies have been developed to incorporate photosensitive groups in nucleotides that can control cellular function or affect biological pathways or gene expression by light (24–29). Of particular interest, such approaches can be used to provide spatiotemporal control of gene activation (24). Here we hypothesized that light triggering can be used to achieve spatiotemporal control of binding of an aptamer injected systemically to its target tissue in vivo, which would have implications for control of delivery of therapeutic aptamers and/or conjugated drugs or drug delivery systems. We designed a photo-triggerable system whereby the aptamer of interest is inactivated by hybridization to a photo-labile complementary oligonucleotide. Upon irradiation, the complementary sequence breaks down, releasing the functional aptamer (Fig. 1). The aptamer of interest is the single-stranded DNA 26-mer aptamer AS1411 (A_{1411}; sequence: 5′-GGT GGT GGT GGT TGT GGT GGT GGT GG-3′) that binds with high affinity and selectivity to nucleolin (30–32), which is overexpressed on the cell membrane of several types of cancer cells, including the 4T1 breast cancer cells used here (33–35). A_{1411} has been used for cancer targeting in vitro and in vivo (35, 36). A complementary photo-triggerable inhibitory oligonucleotide (OliP) was designed [sequence: 5′-CCA CCA//CCA CCA//CAA CCA C-3′, where // indicates photo-labile 1-(2-nitrophenyl)ethyl bonds (37); Scheme S1].

Results

We examined the formation and light-triggered dehybridization of double-stranded A_{1411}/OliP in vitro using Förster resonance energy transfer (FRET). A_{1411} was labeled with a Cy3 fluorophore at the 3′ end (Cy3-A_{1411}) and OliP was modified with a quencher of Cy3 (Iowa Black RQ) at the 5′ end (Q-OliP); the change of FRET signal between the fluorophore and quencher would allow evaluation of the photoactivation process (Fig. 2 *A* and *B*). The addition of Q-OliP to Cy3-A_{1411} in solution quenched the fluorescence of Cy3 due to FRET (Fig. 2*C*), confirming the formation of the A_{1411}/OliP hybrid structure. Irradiation (365 nm light at 5 mW/cm^2) of the Cy3-A_{1411}/Q-OliP hybrid resulted in an increase in fluorescence intensity at the emission wavelength of Cy3 (Fig. 2*D*), indicating release of the Cy3-A_{1411} strand from the hybrid, which peaked in 5 min (Fig. S1). There was no change in fluorescence intensity upon irradiating Cy3-A_{1411} hybridized to a quencher-bearing DNA strand with the same sequence as Q-OliP but without photo-cleavable bonds (Q-Oli; Fig. S2), suggesting that breakage of the photo-labile bonds by light was crucial to the release of the aptamer from the hybrid. Native polyacrylamide gel electrophoresis was performed to further confirm the light-triggered dehybridization of A_{1411}/OliP; ~95% of the OliP was cleaved after 5 min of irradiation (365 nm light at 5 mW/cm^2; Fig. S3).

The ability of A_{1411}/OliP hybrid to target cancer cells was investigated in vitro. Fluorescent Cy3-A_{1411}/OliP was incubated with 4T1 breast cancer cells (nucleolin-positive) at 37 °C for 2 h. Fluorescence microscopy revealed minimal uptake into cells exposed to 0.5 μM Cy3-A_{1411}/OliP compared with cells incubated with free Cy3-A_{1411} (Fig. 3*A*), indicating that hybridization to OliP inhibited

Significance

The importance of this research is in the demonstration of the spatiotemporal regulation of aptamer activity in vitro and in vivo that can be achieved by a photo-triggered strategy. The aptamer's cell-binding capability was blocked by hybridization with a photo-cleavable complementary oligonucleotide. Irradiation at the tumor site liberated the aptamer from the duplex, leading to prolonged intratumoral retention. Furthermore, the relative distribution of the aptamer to the tumor was enhanced in relation to uptake by the liver and kidneys. Our strategy may provide an approach to improving the therapeutic indices of aptamer-based medicines.

Author contributions: L.L., R.T., and D.S.K. designed research; L.L., R.T., H.C., and W.W. performed research; L.L., R.T., R.L., and D.S.K. analyzed data; and L.L., R.T., R.L., and D.S.K. wrote the paper.

The authors declare no conflict of interest.

[1]L.L. and R.T. contributed equally to this work.

[2]To whom correspondence may be addressed. Email: rlanger@mit.edu or daniel.kohane@childrens.harvard.edu.

This article contains supporting information online at www.pnas.org/lookup/suppl/doi:10.1073/pnas.1420105111/-/DCSupplemental.

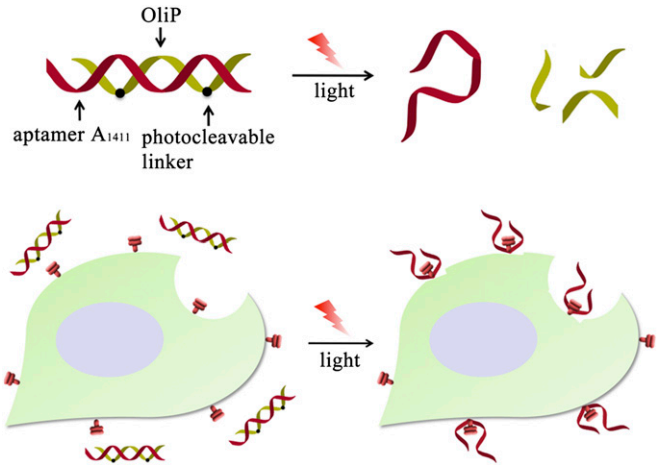

Fig. 1. The AS1411 aptamer (A_{1411}, red DNA strand) is hybridized to a complementary oligonucleotide (OliP, green DNA strand) containing photo-cleavable bonds (black dots). The hybridized complex cannot bind cells. The A_{1411} can be released by light-triggered breakage of the OliP, allowing binding to cell surfaces.

the activity of A_{1411}. Irradiation of Cy3-A_{1411}/OliP (365 nm, 5 min, 5 mW/cm^2) induced cell uptake comparable to that seen with free Cy3-A_{1411}, suggesting that irradiation released functional A_{1411} from the hybrid. Quantitation by flow cytometry revealed that the fluorescence intensity of 4T1 cells incubated with Cy3-A_{1411}/OliP was approximately three times less than that of cells treated with Cy3-A_{1411} ($P < 0.005$; $n = 4$). Upon irradiation (365 nm light at 5 mW/cm^2 for 5 min), the fluorescence intensity of cells incubated with Cy3-A_{1411}/OliP increased ~2.5-fold ($P < 0.005$, $n = 4$), that is, to a level similar to that of cells treated with free A_{1411} (Fig. 3*B*). In contrast, cellular uptake of Cy3-A_{1411}/Oli without photocleavable bonds did not increase upon irradiation (Fig. S4), supporting the view that it was the photocleavable nature of OliP that enabled light-responsive cell binding by A_{1411}/OliP.

Intratumoral photoactivation of A_{1411}/OliP was demonstrated by intravital microscopy (38, 39) in nude mice with 4T1 tumors (diameters ~6–8 mm) on their mammary fat pads. Mice were administered A_{1411} or A_{1411}/OliP (250 nmol/kg) i.v., both labeled with the fluorescent dye Cy3. FITC-dextran (molecular mass ~70 kDa)

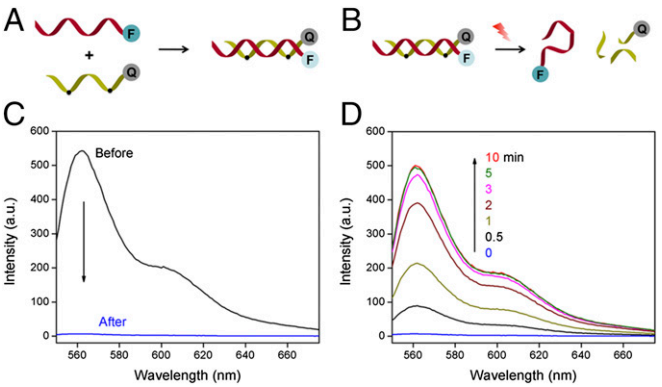

Fig. 2. FRET study of the formation of A_{1411}/OliP and the light-triggered release of A_{1411}. (*A*) Schema of the formation of A_{1411}/OliP FRET pairs through hybridization of fluorophore (F, Cy3)-labeled A_{1411} to quencher (Q, Iowa Black RQ)-labeled OliP. (*B*) Schema of light-triggered release of Cy3-A_{1411} with inhibition of the FRET (i.e., increased fluorescence). (*C*) Fluorescence spectrum of Cy3-A_{1411} before and after hybridization with quencher-labeled OliP. (*D*) Time course of the fluorescence spectrum of A_{1411}/OliP following dehybridization under continuous irradiation (365 nm light at 5 mW/cm^2).

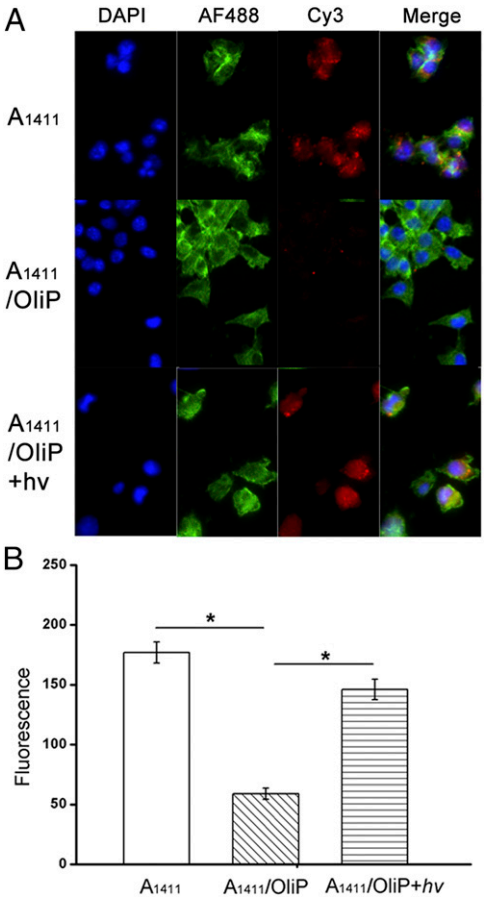

Fig. 3. Photoactivation of Cy3-A_{1411}/OliP in 4T1 cancer cells in vitro. (*A*) Fluorescence images of the 4T1 cells incubated with Cy3-A_{1411}, nonirradiated A_{1411}/OliP, or irradiated Cy3-A_{1411}/OliP (365 nm light at 5 mW/cm^2 for 5 min). (*B*) Flow cytometric quantification of the cells from *A*. Data are means ± SD, $n = 4$, asterisks indicate $P < 0.005$.

was also injected i.v. to highlight the vasculature (40). Injection of free Cy3-A_{1411} resulted in strong extravasated fluorescence in the tumor tissue 10 min after injection. Administration of Cy3-A_{1411}/OliP resulted in minimal fluorescence in the same time frame (Fig. 4). Irradiation of the tumor site (365 nm light at 200 mW/cm^2 for 3 min; see *SI Materials and Methods*, section S6 for the rationales for irradiation timing and Figs. S5 and S6) immediately after injection of Cy3-A_{1411}/OliP resulted in more extravasated fluorescence throughout the tumor tissue compared with that without light irradiation. These results suggest that A_{1411}/OliP could be dehybridized to liberate A_{1411} upon irradiation at the tumor site in vivo.

Fluorescence imaging of tumor sections 2 h postadministration showed distribution of Cy5-A_{1411} throughout the tumor tissue (Fig. 5), whereas A_{1411}/OliP was mainly localized around blood vessels, presumably because of inhibition of the aptamer's binding to cells. [The 2-h time point was selected because pilot studies suggested that free (unbound) A_{1411}/OliP was still present in tumors in large quantity at earlier time points; see also Fig. 6*B*.] When the tumor site was irradiated for 3 min immediately after administration of A_{1411}/OliP, Cy5 fluorescence was found to be distributed throughout the tumor at necropsy 2 h later.

To examine the effect of light triggering on biodistribution, nude mice bearing s.c. 4T1 tumors were administered Cy5-labeled A_{1411} or A_{1411}/OliP i.v. then underwent quantitative whole-body fluorescence imaging (Fig. 6). The tumors were placed at the neck so that signal from the liver and other organs with significant nonspecific uptake would not interfere with signal from the tumor. To

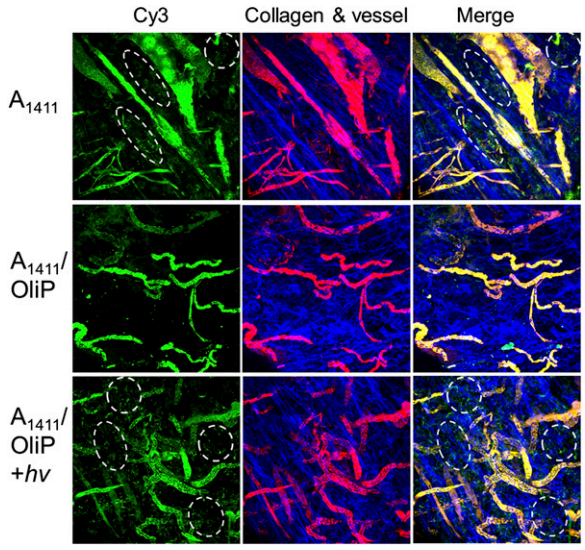

Fig. 4. Representative intravital microscopic images of orthotopic 4T1 tumors 10 min after i.v. administration of Cy3-labeled A_{1411} or A_{1411}/OliP, without or with light triggering at the tumor site (365 nm light at 200 mW/cm^2 for 3 min) immediately after injection. Green, Cy3-labeled A_{1411} or A_{1411}/OliP; red, FITC-dextran (~70 kDa) that demarcates blood vessels; blue, intratumoral collagen matrix; yellow, the localization of A_{1411} or A_{1411}/OliP in blood vessels. The accumulation of A_{1411} and A_{1411}/OliP in extravascular spaces (indicated by white dashed ovals) with light triggering was observed. Two animals were imaged in each group.

minimize autofluorescence, the mice were fed a purified diet for 1 wk before experiments (41). Fluorescence from A_{1411} was readily detected in tumors 2 h after injection (Fig. 6*A*) but not in animals injected with A_{1411}/OliP. Irradiation at the tumor site (365 nm light at 200 mW/cm^2 for 3 min) immediately after i.v. injection of A_{1411}/OliP resulted in strong fluorescence at the tumor site, similar to that in the group receiving A_{1411}, and 1.4-fold higher than that in mice receiving A_{1411}/OliP without irradiation (Fig. 6*B*). The rate of clearance from tumor of A_{1411}/OliP after irradiation ($t_{1/2}$ = 1,124.8 s; Fig. 6*B*) was slower than that of A_{1411}/OliP ($t_{1/2}$ = 977.2 s). Of note, A_{1411}/Oli showed similar intratumoral fluorescence intensity 2 h after administration with and without irradiation (200 mW/cm^2, 3 min) (Fig. S7), suggesting that increased binding of A_{1411}/OliP was due to photo-cleavage of OliP and not a direct effect of irradiation on tissue, such as enhanced capillary permeability. These results suggest that A_{1411} was liberated from the hybrid upon irradiation, rapidly taken up by tumors (Fig. 4), and was retained there. Examination of irradiated H&E-stained sections of tissues (tumors and overlying skin) did not show signs of tissue injury compared with nonirradiated controls (Fig. S8).

Quantitative fluorescence imaging of tissues 2 h after injection showed that the intratumoral fluorescence signal intensity (median radiance) in the light-triggered A_{1411}/OliP group was similar to that in the group treated with free A_{1411} ($P > 0.1$, $n = 5$, Fig. 6 *C* and *D*) and was 2.2-fold higher than that in the group that received A_{1411}/OliP without irradiation ($P < 0.05$, $n = 5$, Fig. 6*C*). Irradiation also increased aptamer accumulation in tumor relative to levels in other organs. The median ratio of liver to tumor radiance in the group that received A_{1411}/OliP with light triggering was 2.5-fold less than that in the group treated with A_{1411} ($P < 0.05$, $n = 5$, Fig. 6*E*). Similarly, the kidney-to-tumor ratio in mice treated with A_{1411}/OliP with irradiation was 63% less than that in the group receiving free A_{1411} ($P < 0.05$).

Discussion

We have demonstrated a strategy for regulating aptamer activity and biodistribution by light triggering. In our design, hybridization with a photo-cleavable complementary oligonucleotide (A_{1411}/OliP) blocked the aptamer's tumor-targeting capability, which was restored when the aptamer was released by photo-triggering. Hybridization also changed the aptamer's biodistribution, possibly by two phenomena: (*i*) enhanced binding to tumor upon irradiation in relation to nonspecific tissue binding, and (*ii*) A_{1411} [and some other aptamers (7)] has a configuration that protects it from nuclease digestion (42) and is reported to have very different biodistribution from other DNA molecules that undergo rapid organ uptake followed by rapid degradation and renal clearance of breakdown products (10, 43, 44). The stability of A_{1411} is greatly diminished by hybridization in A_{1411}/OliP (Fig. S9).

Aptamers can be covalently bound to a wide variety of therapeutic agents, including chemotherapeutics or enzymes (45, 46), siRNA (47, 48), or drug-loaded nanocarriers (36, 49), to provide targeted drug delivery. The spatiotemporal control of drug delivery afforded by our approach may enhance the efficacy and therapeutic index of many drugs. Our strategy involves less synthetic workup than approaches that change oligonucleotide biodistribution via chemical modification (e.g., PEGylation) (14, 50–52).

Although UVA light (320–400 nm) has been widely used for photochemical regulation of biological activities in vitro and in vivo (21–26), UVA light possesses clinical limitations such as limited tissue penetration. Clinical applicability could be enhanced by use of two-photon technology whereby near-infrared light, which can penetrate tissues more deeply, could be used to cleave two-photon photolabile groups (26, 53). Fiberoptic endoscopy could also be used to use UVA light deep within the body (54, 55). Brief irradiation with 365 nm light at low energy is not considered a risk for skin cancer (56, 57).

Materials and Methods

A full description of materials and methods is provided in *SI Materials and Methods*.

A_{1411}/OliP Synthesis. A_{1411}/OliP stock solution was prepared by adding OliP to a solution (PBS, 150 mM NaCl, pH 7.4) of DNA aptamers labeled with a dye with a final ratio of A_{1411}: OliP of 1:1. The solution was annealed and stored at 4 °C overnight to allow full hybridization.

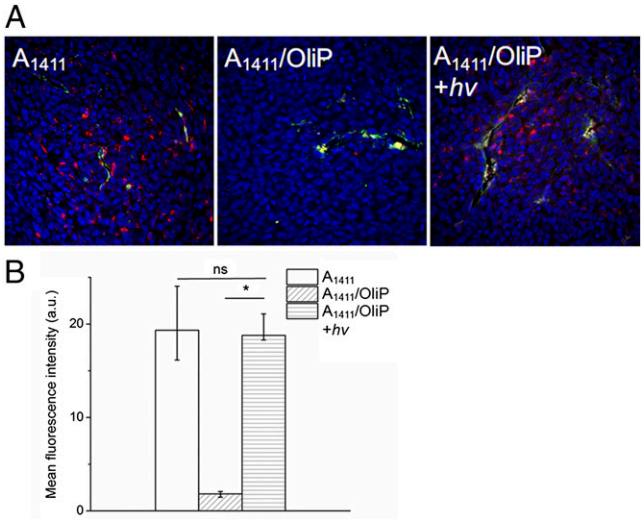

Fig. 5. Intratumoral aptamer distribution. (*A*) Representative fluorescence images of intratumoral distribution of Cy5-labeled A_{1411} and A_{1411}/OliP (red) 2 h after i.v. injection, without or with irradiation (365 nm at 200 mW/cm^2 for 3 min) immediately postinjection. Blue, cell nucleus; green, antibody against CD31 staining blood vessel endothelial cells; yellow, colocalization of red and green. (*B*) Quantitation of the data in *A*. Numeric data are medians ± quartiles; $n = 4$. Asterisk indicates $P < 0.01$. ns, $P > 0.05$.

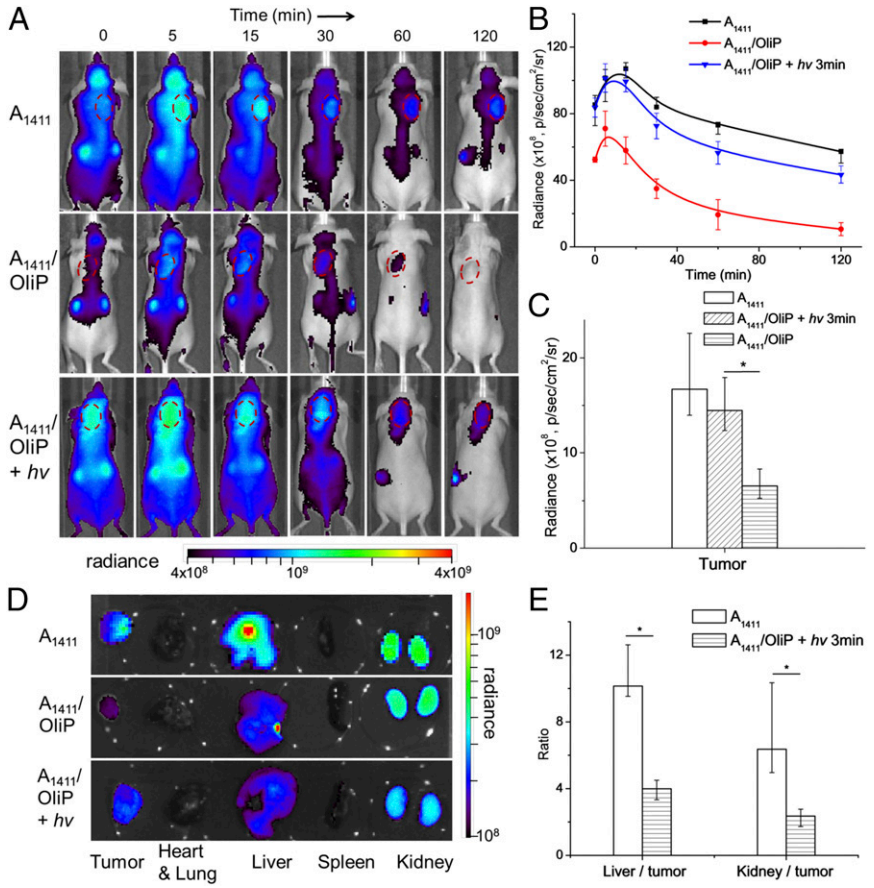

Fig. 6. Effect of light triggering of A_{1411}/OliP on biodistribution. (*A*) Representative whole-body fluorescence images of 4T1 tumor-bearing mice injected i.v. with Cy5-labeled A_{1411} or A_{1411}/OliP without or with subsequent irradiation at the tumor site (365 nm light at 200 mW/cm^2 for 3 min). Tumors are indicated by red dashed circles. (*B*) Time course of intratumoral Cy5 fluorescence over 2 h, derived from integration of the photoradiance [photons per second per square centimeter per steradian (p/s/cm^2/sr)] in *A*. $n = 5$. (*C*) Intratumor accumulation of Cy5 2 h after injection. Data are medians ± quartiles ($n = 5$). Asterisk indicates $P < 0.05$. (*D*) Representative fluorescence images of organs and tumors 2 h after i.v. injection. (*E*) The ratio of photoradiance in livers to that in tumors and kidneys to tumors for mice that received A_{1411} or A_{1411}/OliP with irradiation. Asterisks indicate $P < 0.01$ ($n = 5$ for all groups). Numeric data are medians ± quartiles.

Cellular Uptake Analysis. 4T1 cells were grown in 12-well plates in RPMI-1640 medium, supplemented with 100 units/mL aqueous penicillin G, 100 mg/mL streptomycin, and 10% (wt/wt) FBS (all from Life Technologies) at concentrations to allow 70% confluence in 24 h (i.e., 2×10^4 cells/cm^2). On the day of experimentation, the medium was replaced with Opti-MEM medium (500 mL) containing 0.5 μM Cy3-labeled A_{1411} or A_{1411}/OliP probes with or without light triggering (365 nm light at 5 mW/cm^2 for 5 min). After incubation for 2 h, the cells were washed with PBS (2×500 μL per well) and treated with 0.25% trypsin with EDTA for 5 min (Life Technologies). After the cells were washed with PBS (2×1 mL), they were fixed with 4% (wt/wt) formaldehyde for 10 min at room temperature, washed with PBS (2×1 mL) and stored in 1 mL PBS with 1% (wt/wt) BSA solution at 4 °C for flow cytometry analysis.

The 4T1 Tumor Model and in Vivo Imaging. Immunodeficient 6- to 8-wk-old nu/nu nude mice were purchased from Charles River Laboratories and maintained under pathogen-free conditions for all animal studies. The study protocol was reviewed and approved by the Massachusetts Institute of Technology Committee on Animal Care. For subcutaneous 4T1 tumor models, 4T1 cells were injected in the dorsal aspect of the neck with 1×10^6 cells/0.2 mL in 1:1 (vol/vol) PBS and Matrigel (BD Biosciences). For orthotopic 4T1 tumors, 1×10^5 cells/0.1 mL in HBSS were injected into mouse mammary fat pads. Tumor length and width were measured with calipers, and the tumor volume was calculated using the following equation: tumor volume = length × width × width / 2. Mice whose tumors reached ~100–200 mm^3 were used in subsequent experiments. The mice were injected intravenously (i.v.) with Cy5-labeled A_{1411} or A_{1411}/OliP at an aptamer dose of 250 nmol/kg. In light-triggering experiments, the tumor site was illuminated by UV light for 3 min (365 nm, 200 mW/cm^2) immediately after injection. Whole body fluorescence imaging was performed with an IVIS imaging system (IVIS spectrum, Caliper Life Sciences) with excitation and emission wavelengths of 640 and 680 nm, respectively.

Statistical Analysis. Data which were reasonably normally distributed were described with means and standard deviations and compared with *t* tests. Otherwise, data were presented as median ± quartiles and differences between groups were assessed with a Mann–Whitney *u* test. All data analyses were performed using Origin 8 software.

ACKNOWLEDGMENTS. We thank Dr. Jeffery Wyckoff (Koch Institute) for his assistance with multiphoton intravital microscopy and the histology core facility at Koch Institute for technical support. The work was supported by NIH Grant GM073626.

1. Ellington AD, Szostak JW (1990) In vitro selection of RNA molecules that bind specific ligands. *Nature* 346(6287):818–822.
2. Tuerk C, Gold L (1990) Systematic evolution of ligands by exponential enrichment: RNA ligands to bacteriophage T4 DNA polymerase. *Science* 249(4968): 505–510.
3. Liu J, Cao Z, Lu Y (2009) Functional nucleic acid sensors. *Chem Rev* 109(5):1948–1998.
4. Meyer C, Hahn U, Rentmeister A (2011) Cell-specific aptamers as emerging therapeutics. *J Nucleic Acids* 2011:904750.
5. White RR, Sullenger BA, Rusconi CP (2000) Developing aptamers into therapeutics. *J Clin Invest* 106(8):929–934.
6. Bunka DHJ, Platonova O, Stockley PG (2010) Development of aptamer therapeutics. *Curr Opin Pharmacol* 10(5):557–562.

7. Xing H, Wong NY, Xiang Y, Lu Y (2012) DNA aptamer functionalized nanomaterials for intracellular analysis, cancer cell imaging and drug delivery. *Curr Opin Chem Biol* 16(3-4):429–435.
8. Tan W, Donovan MJ, Jiang J (2013) Aptamers from cell-based selection for bioanalytical applications. *Chem Rev* 113(4):2842–2862.
9. Keefe AD, Pai S, Ellington A (2010) Aptamers as therapeutics. *Nat Rev Drug Discov* 9(7):537–550.
10. Tavitian B, et al. (1998) In vivo imaging of oligonucleotides with positron emission tomography. *Nat Med* 4(4):467–471.
11. Zhao W, et al. (2011) Cell-surface sensors for real-time probing of cellular environments. *Nat Nanotechnol* 6(8):524–531.
12. Schmidt KS, et al. (2004) Application of locked nucleic acids to improve aptamer in vivo stability and targeting function. *Nucleic Acids Res* 32(19):5757–5765.
13. Reyderman L, Stavchansky S (1998) Pharmacokinetics and biodistribution of a nucleotide-based thrombin inhibitor in rats. *Pharm Res* 15(6):904–910.
14. Da Pieve C, Blackshaw E, Missailidis S, Perkins AC (2012) PEGylation and biodistribution of an anti-MUC1 aptamer in MCF-7 tumor-bearing mice. *Bioconjug Chem* 23(7):1377–1381.
15. Mi J, et al. (2010) In vivo selection of tumor-targeting RNA motifs. *Nat Chem Biol* 6(1): 22–24.
16. Henry SP, et al. (2002) Complement activation is responsible for acute toxicities in rhesus monkeys treated with a phosphorothioate oligodeoxynucleotide. *Int Immunopharmacol* 2(12):1657–1666.
17. Sundaram P, Kurniawan H, Byrne ME, Wower J (2013) Therapeutic RNA aptamers in clinical trials. *Eur J Pharm Sci* 48(1-2):259–271.
18. Oney S, et al. (2009) Development of universal antidotes to control aptamer activity. *Nat Med* 15(10):1224–1228.
19. Rusconi CP, et al. (2004) Antidote-mediated control of an anticoagulant aptamer in vivo. *Nat Biotechnol* 22(11):1423–1428.
20. Rusconi CP, et al. (2002) RNA aptamers as reversible antagonists of coagulation factor IXa. *Nature* 419(6902):90–94.
21. Tong R, Chiang HH, Kohane DS (2013) Photoswitchable nanoparticles for in vivo cancer chemotherapy. *Proc Natl Acad Sci USA* 110(47):19048–19053.
22. Tong R, Hemmati HD, Langer R, Kohane DS (2012) Photoswitchable nanoparticles for triggered tissue penetration and drug delivery. *J Am Chem Soc* 134(21):8848–8855.
23. Dvir T, Banghart MR, Timko BP, Langer R, Kohane DS (2010) Photo-targeted nanoparticles. *Nano Lett* 10(1):250–254.
24. Shestopalov IA, Sinha S, Chen JK (2007) Light-controlled gene silencing in zebrafish embryos. *Nat Chem Biol* 3(10):650–651.
25. Brieke C, Rohrbach F, Gottschalk A, Mayer G, Heckel A (2012) Light-controlled tools. *Angew Chem Int Ed Engl* 51(34):8446–8476.
26. Liu Q, Deiters A (2014) Optochemical control of deoxyoligonucleotide function via a nucleobase-caging approach. *Acc Chem Res* 47(1):45–55.
27. Ellis-Davies GCR (2007) Caged compounds: Photorelease technology for control of cellular chemistry and physiology. *Nat Methods* 4(8):619–628.
28. Schroeder A, et al. (2012) Remotely activated protein-producing nanoparticles. *Nano Lett* 12(6):2685–2689.
29. Lovatt D, et al. (2014) Transcriptome in vivo analysis (TIVA) of spatially defined single cells in live tissue. *Nat Methods* 11(2):190–196.
30. Soundararajan S, Chen W, Spicer EK, Courtenay-Luck N, Fernandes DJ (2008) The nucleolin targeting aptamer AS1411 destabilizes Bcl-2 messenger RNA in human breast cancer cells. *Cancer Res* 68(7):2358–2365.
31. Reyes-Reyes EM, Teng Y, Bates PJ (2010) A new paradigm for aptamer therapeutic AS1411 action: Uptake by macropinocytosis and its stimulation by a nucleolin-dependent mechanism. *Cancer Res* 70(21):8617–8629.
32. Soundararajan S, et al. (2009) Plasma membrane nucleolin is a receptor for the anticancer aptamer AS1411 in MV4-11 leukemia cells. *Mol Pharmacol* 76(5):984–991.
33. Ginisty H, Sicard H, Roger B, Bouvet P (1999) Structure and functions of nucleolin. *J Cell Sci* 112(Pt 6):761–772.
34. Hovanessian AG, et al. (2010) Surface expressed nucleolin is constantly induced in tumor cells to mediate calcium-dependent ligand internalization. *PLoS ONE* 5(12): e15787.
35. Tang L, et al. (2012) Aptamer-functionalized, ultra-small, monodisperse silica nanoconjugates for targeted dual-modal imaging of lymph nodes with metastatic tumors. *Angew Chem Int Ed Engl* 51(51):12721–12726.
36. Cao Z, et al. (2009) Reversible cell-specific drug delivery with aptamer-functionalized liposomes. *Angew Chem Int Ed Engl* 48(35):6494–6498.
37. Olejnik J, Krzymanska-Olejnik E, Rothschild KJ (1998) Photocleavable aminotag phosphoramidites for 5′-termini DNA/RNA labeling. *Nucleic Acids Res* 26(15):3572–3576.
38. van de Ven AL, Kim P, Ferrari M, Yun SH (2013) Real-time intravital microscopy of individual nanoparticle dynamics in liver and tumors of live mice. *Nat Protocols Exchange*, 10.1038/protex.2013.049.
39. Jain RK, Munn LL, Fukumura D (2012) Mammary fat pad tumor preparation in mice. *Cold Spring Harbor Protocols* 2012(10):1115–1116.
40. Dvorak HF, Nagy JA, Dvorak JT, Dvorak AM (1988) Identification and characterization of the blood vessels of solid tumors that are leaky to circulating macromolecules. *Am J Pathol* 133(1):95–109.
41. Inoue Y, Izawa K, Kiryu S, Tojo A, Ohtomo K (2008) Diet and abdominal autofluorescence detected by in vivo fluorescence imaging of living mice. *Mol Imaging* 7(1):21–27.
42. Dapić V, et al. (2002) Antiproliferative activity of G-quartet-forming oligonucleotides with backbone and sugar modifications. *Biochemistry* 41(11):3676–3685.
43. Li J, et al. (2014) Aptamer imaging with Cu-64 labeled AS1411: Preliminary assessment in lung cancer. *Nucl Med Biol* 41(2):179–185.
44. Emlen W, Mannik M (1982) Clearance of circulating DNA-anti-DNA immune complexes in mice. *J Exp Med* 155(4):1210–1215.
45. Chen CHB, et al. (2008) Aptamer-based endocytosis of a lysosomal enzyme. *Proc Natl Acad Sci USA* 105(41):15908–15913.
46. Huang YF, et al. (2009) Molecular assembly of an aptamer-drug conjugate for targeted drug delivery to tumor cells. *ChemBioChem* 10(5):862–868.
47. Dassie JP, et al. (2009) Systemic administration of optimized aptamer-siRNA chimeras promotes regression of PSMA-expressing tumors. *Nat Biotechnol* 27(9):839–849.
48. McNamara JO, 2nd, et al. (2006) Cell type-specific delivery of siRNAs with aptamer-siRNA chimeras. *Nat Biotechnol* 24(8):1005–1015.
49. Kim E, et al. (2010) Prostate cancer cell death produced by the co-delivery of Bcl-xL shRNA and doxorubicin using an aptamer-conjugated polyplex. *Biomaterials* 31(16): 4592–4599.
50. Ng EWM, et al. (2006) Pegaptanib, a targeted anti-VEGF aptamer for ocular vascular disease. *Nat Rev Drug Discov* 5(2):123–132.
51. Hicke BJ, et al. (2006) Tumor targeting by an aptamer. *J Nucl Med* 47(4):668–678.
52. Boomer RM, et al. (2005) Conjugation to polyethylene glycol polymer promotes aptamer biodistribution to healthy and inflamed tissues. *Oligonucleotides* 15(3):183–195.
53. Pawlicki M, Collins HA, Denning RG, Anderson HL (2009) Two-photon absorption and the design of two-photon dyes. *Angew Chem Int Ed Engl* 48(18):3244–3266.
54. Weissleder R (2001) A clearer vision for in vivo imaging. *Nat Biotechnol* 19(4):316–317.
55. Yelin D, et al. (2006) Three-dimensional miniature endoscopy. *Nature* 443(7113): 765–765.
56. Bowden GT (2004) Prevention of non-melanoma skin cancer by targeting ultraviolet-B-light signalling. *Nat Rev Cancer* 4(1):23–35.
57. de Gruijl FR, et al. (1993) Wavelength dependence of skin cancer induction by ultraviolet irradiation of albino hairless mice. *Cancer Res* 53(1):53–60.